Efficient method for analyzing multiple circular cylindrical nanoparticles on a substrate

Xun Lu and Ya Yan Lu*

Department of Mathematics, City University of Hong Kong, Kowloon, Hong Kong

compiled: March 3, 2016

Due to the existing nanofabrication techniques, many metallic or dielectric nanoparticles are cylindrical objects with top and bottom surfaces parallel to a substrate and side boundaries perpendicular to the substrate. In this paper, we develop a relatively simple and efficient semi-analytic method for analyzing the scattering of light by a set of circular cylindrical objects (of finite height) in a layered background. The method relies on expanding the field in one-dimensional modes in layered regions where the material properties change with one spatial variable only, to establish a linear system on the boundaries separating the layered regions. Although the "expansion coefficients" are two-dimensional (2D) functions, they satisfy scalar 2D Helmholtz equations which have analytic solutions due to the special geometry. The method is used to analyze dielectric and metallic circular cylindrical nanoparticles on a substrate or in free space.

1. Introduction

In recent years, metallic nanoparticles of various size and shape have been intensively studied, mainly due to the many applications related to the strongly enhanced near-field and the localized surface plasmon resonances [1–6]. Numerical methods are indispensible in the studies of nanoparticles, since analytic solutions are only available for a few special cases such as spherical particles. Standard numerical methods for solving Maxwell's equations, such as the finite-difference time-domain (FDTD) method [7] and the frequency-domain finite element method (FEM) [8], are widely used, but they often take too much computation time, when nanoparticles of various geometric parameters are analyzed. FDTD must use a small grid size to catch rapid field variations and resolve curved interfaces, must use a small time step to maintain stability, and must also properly model dispersive media. FEM usually gives rise to large, complex and indefinite linear systems that are expensive to solve. The boundary element method [9–11] is another important method, but it is somewhat complicated to implement if the background is a layered medium. Clearly, to realize new and practical applications based on metallic nanoparticles, a more efficient numerical or semi-analytic method is highly desired.

By taking advantage of some geometric features for a family of structures, it is often possible to develop special computational methods that are much more efficient than the general numerical methods. As a result of the existing nanofabrication techniques, such as the electron beam lithography, many nanoparticles are cylindrical objects, that is, their top and bottom surfaces are parallel to the substrate and their side surfaces are perpendicular to the substrate. In that case, the overall structure involving the nanoparticles, the substrate and the surrounding media, can be divided into a number of z-invariant layers, where z is the spatial variable perpendicular to the substrate. Therefore, the problem can be analyzed by some kind of numerical modal method, such as the Fourier modal method [12–15] and the finite element modal method [16]. A numerical modal method is a semi-analytic method, since the field in each z-invariant layer is expanded as a sum of the related eigenmodes without a discretization of the z variable. Unfortunately, the numerical modal methods are not particularly efficient, since a large number of eigenmodes are needed, and they are full vectorial modes depending on the two transverse variables and are expensive to calculate.

In a recent work [17], we developed a vertical mode expansion method (VMEM) to analyze circular apertures in a metallic film. In contrast to the modal method, VMEM divides the whole structure into regions where the material properties depend only on z and expands the field in each of these regions. The method has been extended to handle cylindrical objects (such as metallic nanoparticles) with arbitrary cross sections [18]. So far, VMEM has only been implemented for structures with a single cylindrical object. In this paper, we implement a VMEM to analyze a finite number of circular cylindrical nanoparticles on a substrate. The single cylinder case studied in [17] has a rotational symmetry, and can be efficiently solved by separating the angle variable in a cylindrical coordinate system. Such a separation of variables is not possible for the more general problem involving multiple cylinders, but fortunately, some analytic soutions are still available. Our method is related to the early work of Boscolo and Midrio [19] on photonic

* Corresponding author: mayylu@cityu.edu.hk

crystal slabs, but also has a number of important differences. In the following sections, we present our method and validate the method by numerical examples.

2. Problem formulation

We consider a finite number of circular cylindrical objects in a layered background. A special case involving three cylinders on a substrate is shown in Fig. 1. Let $\{x, y, z\}$ be a Cartesian coordinate system where z

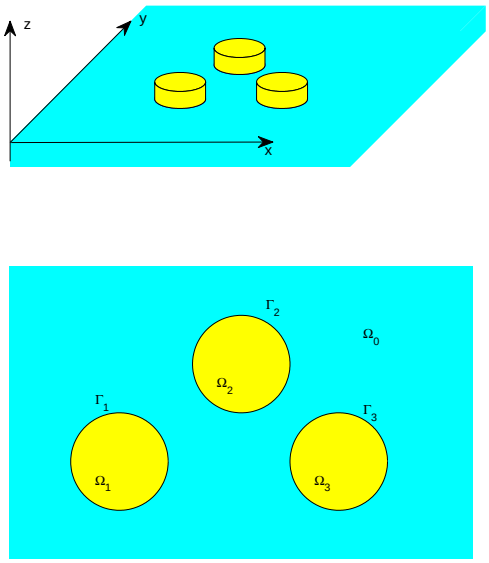

Fig. 1. Top panel: three circular cylinders on a substrate. Bottom panel: horizontal cross section of the structure.

is identified as the vertical variable, the cylindrical objects are assumed to have horizontal cross sections Ω_l for $1 \le l \le l_*$, where $l_* \ge 1$ is the total number of objects, and

$$\Omega_l = \{\boldsymbol{r} = (x, y) \ : \ |\boldsymbol{r} - \boldsymbol{c}_l| < a_l\}$$

is a circular disk with center $\boldsymbol{c}_l$ and radius a_l. The infinite domain outside all Ω_l $(1 \le l \le l_*)$ is denoted as

$$\Omega_0 = \{\boldsymbol{r} \ : \ |\boldsymbol{r} - \boldsymbol{c}_l| > a_l \text{ for } 1 \le l \le l_*\}.$$

The horizontal cross section of the structure with three cylinders is shown in the bottom panel of Fig. 1. For each Ω_l $(0 \le l \le l_*)$, we define a three-dimensional (3D) region

$$S_l = \{(x, y, z) \ : \ (x, y) \in \Omega_l, \ -\infty < z < \infty\},$$

and assume that the relative permittivity ε and relative permeability μ depend only on z in each S_l, that is,

$$\varepsilon = \varepsilon^{(l)}(z), \quad \mu = \mu^{(l)}(z), \quad (x, y, z) \in S_l.$$

It is further assumed that the horizontal variation of the entire structure is limited to the finite z-interval given by $0 < z < D$, and the media in the top $(z > D)$ and bottom $(z < 0)$ are homogeneous. We have

$$\begin{aligned} \varepsilon &= \varepsilon_t, \quad \mu = \mu_t, \quad z > D, \\ \varepsilon &= \varepsilon_b, \quad \mu = \mu_b, \quad z < 0, \end{aligned}$$

where ε_t, μ_t, ε_b and μ_b are positive constants.

If we consider some circular cylindrical nanoparticles on an infinitely-thick substrate, then the lower half space $(z < 0)$ corresponds to the substrate, $\boldsymbol{c}_l$ and a_l are the horizontal center and radius of the lth nanoparticle respectively, and D is the height of the tallest nanoparticle. The nanoparticles could have different material properties, different radii and different heights. Furthermore, the structures could have more complicated vertical profiles, for example, an adhesion layer between the nanoparticle and the substrate can be included. Notice that the structure described above could also represent a metallic film or a dielectric slab with a finite number of circular holes.

Our objective is to analyze the scattering of an incident plane wave by such a multiply-layered structure with circular cylindrical inclusions. We specify an incident wave in the top homogeneous medium, and assume the wave vector is $(\alpha, \beta, -\gamma)$, where α and β are real,

$$\gamma = \sqrt{k_0^2 \varepsilon_t \mu_t - \alpha^2 - \beta^2}$$

is positive, and k_0 is the free space wavenumber. The problem is considered in the frequency-domain. The time dependence is assumed to be $e^{-\mathrm{i}\omega t}$, where ω is the angular frequency. The electromagnetic field satisfies the following linear Maxwell's equations

$$\nabla \times \mathbf{E} = \mathrm{i} k_0 \mu \mathbf{H}, \quad \nabla \times \mathbf{H} = -\mathrm{i} k_0 \varepsilon \mathbf{E}, \qquad (1)$$

where $\mathbf{E}$ is the electric field and $\mathbf{H}$ is a scaled magnetic field (the magnetic field multiplied by the free space impedance).

3. Vertical mode expansions

The foundation of VMEM is a set of expressions for a general electromagnetic field in an arbitrary one-dimensional (1D) medium, i.e. a layered medium where ε and μ depend only on one spatial variable z. The expressions can be obtained by expanding the field in transverse electric (TE) and transverse magnetic (TM) modes with 1D profiles that are functions of z only. For that purpose, it is necessary to truncate z with perfectly matched layers (PMLs), so that the outgoing radiation condition (for $z \to \pm\infty$) are approximately satisfied and the expansions are discrete sums. For region S_l, we denote the 1D modes, i.e., the vertical modes, as $\phi_j^{(l,p)}(z)$, where l is the location index, $p \in \{e, h\}$ is the polarization index, and $j \in \{1, 2, ...\}$ is the mode index. The corresponding propagation constant is denoted as $\eta_j^{(l,p)}$. As in standard theory on planar waveguides, $\phi_j^{(l,p)}(z)$ and

$\eta_j^{(l,p)}$ satisfy an eigenvalue equation for z in the truncated interval. More details are given in [17].

For our problem stated in the previous section, the total field is not outgoing as $z \to +\infty$, since there is an incident wave coming down from the top. This leads to a contradiction with the use of PMLs for truncating the z variable. It is impossible to simply expand the difference between the total field $\{\mathbf{E}, \mathbf{H}\}$ and the incident wave, since that difference does not satisfy homogeneous Maxwell's equations (1). The approach developed in [17] is to expand $\{\mathbf{E}-\mathbf{E}^{(l)}, \mathbf{H}-\mathbf{H}^{(l)}\}$ in S_l, where $\{\mathbf{E}^{(l)}, \mathbf{H}^{(l)}\}$ is the solution of a hypothetical 1D problem where $\varepsilon = \varepsilon^{(l)}(z)$ and $\mu = \mu^{(l)}(z)$ for all (x, y).

The vertical mode expansions for the two z components in S_l are given as

$$H_z = H_z^{(l)} + \frac{1}{\mu^{(l)}} \sum_{j=1}^{\infty} [\eta_j^{(l,e)}]^2 \phi_j^{(l,e)} V_j^{(l,e)}, \tag{2}$$

$$E_z = E_z^{(l)} + \frac{1}{\varepsilon^{(l)}} \sum_{j=1}^{\infty} [\eta_j^{(l,h)}]^2 \phi_j^{(l,h)} V_j^{(l,h)}, \tag{3}$$

where $H_z^{(l)}$ and $E_z^{(l)}$ are the z components of the 1D solution $\{\mathbf{E}^{(l)}, \mathbf{H}^{(l)}\}$, and $V_j^{(l,p)}$ (for $p \in \{e, h\}$ and $j = 1$, 2, ...) are unknown expansion "coefficients". In fact, $V_j^{(l,p)}$ are functions of x and y satisfying the following two-dimensional (2D) Helmholtz equations

$$\frac{\partial^2 V_j^{(l,p)}}{\partial x^2} + \frac{\partial^2 V_j^{(l,p)}}{\partial y^2} + [\eta_j^{(l,p)}]^2 V_j^{(l,p)} = 0 \quad \text{in} \quad \Omega_l. \tag{4}$$

Notice that H_z and E_z are expanded in TE and TM modes, respectively. Although the expansions (2) and (3) involve 2D unknown functions, we emphasize that the Helmholtz equations for $V_j^{(l,p)}$ are independent of each other. In the sections below, we show that it is only necessary to solve $V_j^{(l,p)}$ on the boundary of Ω_l.

It is helpful to compare the expansions (2) and (3) with those used in a numerical modal method. In the latter case, the field in a z-invariant layer is expanded in 2D modes whose mode profiles are functions of x and y, and the dependence on z can be written down analytically with only two unknown coefficients for each mode. These 2D modes are full vectorial and difficult to solve. More importantly, in order to accurately approximate the field, a large number of 2D modes must be retained. In contrast, the field can be well approximated using only a relatively small number of vertical modes in expansions (2) and (3).

The other field components can also be expanded in the 1D vertical modes. For that purpose, we write down the expansions for the field components along an arbitrary direction τ, where τ and ν are a pair of orthogonal unit vectors in the horizontal plane, satisfying

$$\tau = (-\nu_y, \nu_x), \quad \nu = (\nu_x, \nu_y).$$

The τ components in S_l can be expanded as

$$H_\tau = H_\tau^{(l)} + \frac{1}{\mu^{(l)}} \sum_{j=1}^{\infty} \frac{d\phi_j^{(l,e)}}{dz} \frac{\partial V_j^{(l,e)}}{\partial \tau} + \mathsf{i} k_0 \sum_{j=1}^{\infty} \phi_j^{(l,h)} \frac{\partial V_j^{(l,h)}}{\partial \nu}, \tag{5}$$

$$E_\tau = E_\tau^{(l)} + \frac{1}{\varepsilon^{(l)}} \sum_{j=1}^{\infty} \frac{d\phi_j^{(l,h)}}{dz} \frac{\partial V_j^{(l,h)}}{\partial \tau} - \mathsf{i} k_0 \sum_{j=1}^{\infty} \phi_j^{(l,e)} \frac{\partial V_j^{(l,e)}}{\partial \nu}, \tag{6}$$

where $H_\tau^{(l)}$ and $E_\tau^{(l)}$ are the τ components of the 1D solution mentioned above, ∂_τ and ∂_ν are the directional derivative operators. A detailed derivation for equations (2)-(6) can be found in [17].

The expansions (2), (3), (5) and (6) are valid for any $\mathbf{r} \in \Omega_l$. They are still valid if we let $\mathbf{r}$ tend to Γ_l, i.e., the boundary of Ω_l. In that case, we let $\nu = \nu(\mathbf{r})$ be a unit normal vector of Γ_l at $\mathbf{r}$. Notice that for $1 \le l \le l_*$, Γ_l is the circle with center $\mathbf{c}_l$ and radius a_l, and we let ν be the outward unit normal vector. For the exterior domain Ω_0, its boundary $\Gamma_0 = \bigcup_{l=1}^{l_*} \Gamma_l$ is the union of these l_* circles. The unit normal vector of Γ_0 is taken to be the same unit normal vector of Γ_l for $1 \le l \le l_*$.

4. Dirichlet-to-Neumann maps

In order to determine the unknown functions $V_j^{(l,p)}$ defined on Ω_l, we will set up a linear system of equations for $V_j^{(l,p)}$ on Γ_l in Section 5. The system is obtained from the continuity conditions of H_z, E_z, H_τ and E_τ, where τ and ν are unit tangential and normal vectors on Γ_l. From (5) and (6), it is clear that we need to express $\partial_\nu V_j^{(l,p)}$ and $\partial_\tau V_j^{(l,p)}$ in terms of $V_j^{(l,p)}$ on Γ_l.

In the exterior domain Ω_0, $V_j^{(0,p)}$ satisfies the Helmholtz equation (4) for $l = 0$ and a radiation condition at infinity. On the boundary Γ_0, the function $V_j^{(0,p)}$ and its normal derivative $\partial_\nu V_j^{(0,p)}$ are related by an operator $\Lambda_j^{(0,p)}$, the so-called Dirichlet-to-Neumann (DtN) map [20], in a simple linear form:

$$\Lambda_j^{(0,p)} V_j^{(0,p)} = \partial_\nu V_j^{(0,p)} \quad \text{on} \quad \Gamma_0. \tag{7}$$

If the boundary Γ_0 is discretized, we can approximate $\Lambda_j^{(0,p)}$ by a matrix.

For $1 \le l \le l_*$, we discretize the circle Γ_l by M_l points. The boundary Γ_0 is the union of these l_* circles and is discretized by the same set of points on all l_* circles. The total number of discretization points for $\partial\Omega_0$ is $M = \sum_{l=1}^{l_*} M_l$. We denote the function $V_j^{(0,p)}$ at these M

points by a column vector

$$\boldsymbol{v}_j^{(0,p)} = \begin{bmatrix} \boldsymbol{u}_j^{(1,p)} \\ \boldsymbol{u}_j^{(2,p)} \\ \vdots \\ \boldsymbol{u}_j^{(l_*,p)} \end{bmatrix}, \tag{8}$$

where the block $\boldsymbol{u}_j^{(l,p)}$ is a column vector of length M_l for $V_j^{(0,p)}$ at the M_l points on Γ_l. Similarly, we have $\partial_\nu \boldsymbol{v}_j^{(0,p)}$ and $\partial_\nu \boldsymbol{u}_j^{(l,p)}$ for $\partial_\nu V_j^{(0,p)}$ at the discretization points on Γ_0 and Γ_l, respectively. We approximate the DtN map $\Lambda_j^{(0,p)}$ by an $M \times M$ matrix $\boldsymbol{\Lambda}_j^{(0,p)}$, such that

$$\boldsymbol{\Lambda}_j^{(0,p)} \boldsymbol{v}_j^{(0,p)} = \partial_\nu \boldsymbol{v}_j^{(0,p)}. \tag{9}$$

To find the matrix DtN map $\boldsymbol{\Lambda}_j^{(0,p)}$, we notice that $V_j^{(0,p)}$ has the following cylindrical wave expansion

$$V_j^{(0,p)}(\boldsymbol{r}) = \sum_{l=1}^{l_*} \sum_{m=-\infty}^{\infty} b_{lm} H_m^{(1)}(\eta_j^{(0,p)} r_l)\, e^{\mathrm{i}m\theta_l} \tag{10}$$

in Ω_0, where $r_l = r_l(\boldsymbol{r})$ and $\theta_l = \theta_l(\boldsymbol{r})$ are the magnitude and polar angle of $\boldsymbol{r} - \boldsymbol{c}_l$, $\boldsymbol{c}_l$ is the center of the disk Ω_l, $H_m^{(1)}$ is the Hankel function of first kind and order m, b_{lm} are unknown coefficients. Since the boundary Γ_l is discretized by M_l points, we truncate the sum over m in Eq. (10) to $-M_l/2 \le m \le M_l/2 - 1$ if M_l is even, or $-(M_l-1)/2 \le m \le (M_l-1)/2$ if M_l is odd. Evaluating the truncated version of Eq. (10) at the M points on Γ_0, we get a matrix $\mathbf{D}$ such that

$$\boldsymbol{v}_j^{(0,p)} = \mathbf{D}\boldsymbol{b},$$

where $\boldsymbol{b}$ is a column vector for coefficients b_{lm}, l ranges from 1 to l_*, and m takes M_l values for each l. We can also evaluate the normal derivative of $V_j^{(0,p)}$ at the M points on Γ_0 from the trancated version of Eq. (10), and obtain a matrix $\mathbf{N}$ satisfying

$$\partial_\nu \boldsymbol{v}_j^{(0,p)} = \mathbf{N}\boldsymbol{b}$$

Therefore, a matrix approximation of the DtN map is given by

$$\boldsymbol{\Lambda}_j^{(0,p)} = \mathbf{N}\mathbf{D}^{-1}. \tag{11}$$

For $1 \le l \le l_*$ and the function $V_j^{(l,p)}$ satisfying Eq. (4) in Ω_l, the DtN map $\Lambda_j^{(l,p)}$ can be constructed from the expansion

$$V_j^{(l,p)}(\boldsymbol{r}) = \sum_{m=-\infty}^{\infty} c_m J_m(\eta_j^{(l,p)} r_l) e^{\mathrm{i}m\theta_l}, \quad \boldsymbol{r} \in \Omega_l, \tag{12}$$

where J_m is the Bessel function of first kind and order m. Retaining M_l terms in Eq. (12), evaluating $V_j^{(l,p)}$ and $\partial_\nu V_j^{(l,p)}$ at the M_l points on Γ_l, we obtain a matrix DtN map $\boldsymbol{\Lambda}_j^{(l,p)}$ such that

$$\boldsymbol{\Lambda}_j^{(l,p)} \boldsymbol{v}_j^{(l,p)} = \partial_\nu \boldsymbol{v}_j^{(l,p)}. \tag{13}$$

There is also a need to relate the tangential derivative of $V_j^{(l,p)}$ to itself on Γ_l. For $1 \le l \le l_*$, Γ_l is a circle, the tangential derivative can be evaluated by the Fourier pseudospectral method [21]. This gives rise to the so-called differentiation matrix $\mathbf{T}_l$ (an $M_l \times M_l$ matrix), such that

$$\mathbf{T}_l \boldsymbol{v}_j^{(l,p)} = \partial_\tau \boldsymbol{v}_j^{(l,p)}, \tag{14}$$

where $\partial_\tau \boldsymbol{v}_j^{(l,p)}$ denotes the column vector for $\partial_\tau V_j^{(l,p)}$ at the M_l points on $\partial\Omega_l$. Notice that $\mathbf{T}_l$ is independent of indices j and p. For the exterior doamin Ω_0, since Γ_0 is just the union of l_* circles, we have an $M \times M$ matrix $\mathbf{T}_0$ satisfying Eq. (14) for $l = 0$ and it is given by

$$\mathbf{T}_0 = \begin{bmatrix} \mathbf{T}_1 & & & \\ & \mathbf{T}_2 & & \\ & & \ddots & \\ & & & \mathbf{T}_{l_*} \end{bmatrix}. \tag{15}$$

5. Linear system

In an actual implementation of VMEM, the variable z is first truncated by PMLs, then discretized by a Chebyshev pesudospectral method [21] that solves the vertical modes $\phi_j^{(l,p)}$. This leads to N numerical TE modes and N numerical TM modes, where N is the number of discretization points for z. The index j in Eqs. (2), (3), (5) and (6) now ranges from 1 to N. We assume z is discretized as z_i for $1 \le i \le N$.

A linear system for $V_j^{(l,p)}$ on Γ_l can be established from the continuity of H_z, E_z, H_τ and E_τ on the vertical boundary of S_l, i.e.,

$$\Pi_l = \{(x, y, z) \ : \ (x, y) \in \Gamma_l, \ -\infty < z < \infty\}.$$

In the discrete version, this is a system for $\boldsymbol{v}_j^{(l,p)}$, $0 \le l \le l_*$, $p \in \{e, h\}$ and $1 \le j \le N$. For a fixed $l \ge 1$, we arrange the vectors $\boldsymbol{v}_j^{(l,p)}$ in one large column vector as

$$\boldsymbol{v}^{(l)} = \begin{bmatrix} \boldsymbol{v}^{(l,e)} \\ \boldsymbol{v}^{(l,h)} \end{bmatrix}, \quad \boldsymbol{v}^{(l,p)} = \begin{bmatrix} \boldsymbol{v}_1^{(l,p)} \\ \boldsymbol{v}_2^{(l,p)} \\ \vdots \\ \boldsymbol{v}_N^{(l,p)} \end{bmatrix}, \quad p \in \{e, h\}. \tag{16}$$

The vector $\boldsymbol{v}_j^{(0,p)}$ is first decomposed as $\boldsymbol{u}_j^{(l,p)}$ for $1 \le l \le l_*$ following Eq. (8), then the vectors $\boldsymbol{u}_j^{(l,p)}$ for each l are organized as one vector $\boldsymbol{u}^{(l)}$ using the same ordering

of Eq. (16). The final linear system can be written as

$$\mathbf{A}\begin{bmatrix}\boldsymbol{v}^{(1)}\\ \boldsymbol{v}^{(2)}\\ \vdots\\ \boldsymbol{v}^{(l_*)}\\ \boldsymbol{u}^{(1)}\\ \boldsymbol{u}^{(2)}\\ \vdots\\ \boldsymbol{u}^{(l_*)}\end{bmatrix}=\begin{bmatrix}\boldsymbol{b}^{(1)}\\ \boldsymbol{b}^{(2)}\\ \boldsymbol{b}^{(3)}\\ \vdots\\ \boldsymbol{b}^{(l_*)}\end{bmatrix}. \tag{17}$$

In Eq. (17) and for $1 \le l \le l_*$, the rows corresponding to the right hand side $\boldsymbol{b}^{(l)}$ are related to the continuity conditions enforced on Π_l. For a function ϕ given on Π_l, we define a vector

$$\vec{\phi}|_{\Pi_l}=\begin{bmatrix}\vec{\phi}_1|_{\Pi_l}\\ \vec{\phi}_2|_{\Pi_l}\\ \vdots\\ \vec{\phi}_N|_{\Pi_l}\end{bmatrix},$$

where $\vec{\phi}_i|_{\Pi_l}$ is a column vector of ϕ for $z = z_i$ and $\boldsymbol{r}$ being the M_l points of Γ_l. Using this notation, the vector $\boldsymbol{b}^{(l)}$ in the right hand side of Eq. (17) can be written as

$$\boldsymbol{b}^{(l)}=\begin{bmatrix}\boldsymbol{b}_1^{(l)}\\ \boldsymbol{b}_2^{(l)}\\ \boldsymbol{b}_3^{(l)}\\ \boldsymbol{b}_4^{(l)}\end{bmatrix}=\begin{bmatrix}\vec{H}_z^{(0)}|_{\Pi_l}-\vec{H}_z^{(l)}|_{\Pi_l}\\ \vec{E}_z^{(0)}|_{\Pi_l}-\vec{E}_z^{(l)}|_{\Pi_l}\\ \vec{H}_\tau^{(0)}|_{\Pi_l}-\vec{H}_\tau^{(l)}|_{\Pi_l}\\ \vec{E}_\tau^{(0)}|_{\Pi_l}-\vec{E}_\tau^{(l)}|_{\Pi_l}\end{bmatrix}, \tag{18}$$

where $H_z^{(0)}$ and $H_z^{(l)}$ are the z component of the magnetic field of the 1D solutions in regions S_0 and S_l, respectively.

On Π_l, there are NM_l discretization points corresponding to M_l points on Γ_l and N points for z. Since H_z is continuous on Π_l, its interior limit from S_l, evaluated by Eq. (2), must be identical to its exterior limit from S_0, evaluated by Eq. (2) with l replaced by 0. Writing down this condition for all NM_l points, we have

$$\mathbf{F}^{(l,e)}\otimes\mathbf{I}_{M_l}\,\boldsymbol{v}^{(l,e)}-\mathbf{F}^{(0,e)}\otimes\mathbf{I}_{M_l}\,\boldsymbol{u}^{(l,e)}=\boldsymbol{b}_1^{(l)}, \tag{19}$$

where $\boldsymbol{b}_1^{(l)}$ is given in (18), $\mathbf{I}_{M_l}$ is the $M_l \times M_l$ identity matrix, $\mathbf{F}^{(l,e)}$ is an $N \times N$ matrix with its (i,j) entry given by

$$\mathbf{F}^{(l,e)}(i,j)=\frac{1}{\mu^{(l)}(z_i)}[\eta_j^{(l,e)}]^2\phi_j^{(l,e)}(z_i),$$

$\mathbf{F}^{(0,e)}$ is defined as $\mathbf{F}^{(l,e)}$ with l replaced by 0, $\otimes$ denotes the matrix Kronecker product, i.e., if $\mathbf{B}$ is a matrix with (i,j) entry b_{ij}, then $\mathbf{B}\otimes\mathbf{C}$ is a block matrix with (i,j) block $b_{ij}\mathbf{C}$. Similarly, the continuity of E_z gives us

$$\mathbf{F}^{(l,h)}\otimes\mathbf{I}_{M_l}\,\boldsymbol{v}^{(l,h)}-\mathbf{F}^{(0,h)}\otimes\mathbf{I}_{M_l}\,\boldsymbol{u}^{(l,h)}=\boldsymbol{b}_2^{(l)}, \tag{20}$$

where $\mathbf{F}^{(l,h)}$ is an $N \times N$ matrix with (i,j) entry

$$\mathbf{F}^{(l,h)}(i,j)=\frac{1}{\varepsilon^{(l)}(z_i)}[\eta_j^{(l,h)}]^2\phi_j^{(l,h)}(z_i),$$

$\mathbf{F}^{(0,h)}$ is similarly defined, and $\boldsymbol{b}_2^{(l)}$ is given in (18).

The continuity conditions for H_τ and E_τ are more tedious to write down. The tangential and normal derivatives of $V_j^{(l,p)}$ and $V_j^{(0,p)}$ must be expressed using the differentiation matrices and the DtN maps. For $l > 0$, we have the tangential differentiation matrix $\mathbf{T}_l$ and the interior DtN map $\mathbf{\Lambda}_j^{(l,p)}$. For the exterior DtN map $\mathbf{\Lambda}_j^{(0,p)}$, we follow the decomposition of $\boldsymbol{v}_j^{(0,p)}$ given in Eq. (8), and rewrite it in block form as

$$\mathbf{\Lambda}_j^{(0,p)}=\begin{bmatrix}\mathbf{M}_{j,1}^{(1,p)} & \mathbf{M}_{j,2}^{(1,p)} & \dots & \mathbf{M}_{j,l_*}^{(1,p)}\\ \mathbf{M}_{j,1}^{(2,p)} & \mathbf{M}_{j,2}^{(2,p)} & \dots & \mathbf{M}_{j,l_*}^{(2,p)}\\ \vdots & \vdots & & \vdots\\ \mathbf{M}_{j,1}^{(l_*,p)} & \mathbf{M}_{j,2}^{(l_*,p)} & \dots & \mathbf{M}_{j,l_*}^{(l_*,p)}\end{bmatrix}. \tag{21}$$

That is, the (l,m) block of $\mathbf{\Lambda}_j^{(0,p)}$ is denoted as $\boldsymbol{M}_{j,m}^{(l,p)}$ and it is an $M_l \times M_m$ matrix.

At the NM_l points on Π_l, the continuity condition of H_τ can be written as

$$\mathbf{G}^{(l,e)}\otimes\mathbf{T}_l\,\boldsymbol{v}^{(l,e)}+\mathbf{\Phi}^{(l,h)}\boldsymbol{v}^{(l,h)}-\mathbf{G}^{(0,e)}\otimes\mathbf{T}_l\,\boldsymbol{u}^{(l,e)}-\sum_{m=1}^{l_*}\mathbf{\Psi}_m^{(l,h)}\boldsymbol{u}^{(m,h)}=\boldsymbol{b}_3^{(l)}, \tag{22}$$

where $\mathbf{G}^{(l,e)}$ is an $N \times N$ matrix with (i,j) entry given by

$$\mathbf{G}^{(l,e)}(i,j)=\frac{1}{\mu^{(l)}(z_i)}\frac{d\phi_j^{(l,e)}}{dz}(z_i),$$

$\mathbf{G}^{(0,e)}$ is similarly defined, $\mathbf{\Phi}^{(l,h)}$ is an $(NM_l)\times(NM_l)$ matrix, or $N\times N$ block matrix, with its (i,j) block given by

$$\mathbf{\Phi}^{(l,h)}(i,j)=\mathrm{i}k_0\phi_j^{(l,h)}(z_i)\mathbf{\Lambda}_j^{(l,h)}, \tag{23}$$

$\mathbf{\Psi}_m^{(l,h)}$ is an $NM_l\times NM_m$ matrix, or $N\times N$ block matrix with its (i,j) block given by

$$\mathbf{\Psi}_m^{(l,h)}(i,j)=\mathrm{i}k_0\phi_j^{(0,h)}(z_i)\mathbf{M}_{j,m}^{(l,h)}. \tag{24}$$

Finally, the continuity condition of E_τ at the NM_l points on Π_l gives

$$\mathbf{G}^{(l,h)}\otimes\mathbf{T}_l\,\boldsymbol{v}^{(l,h)}-\mathbf{\Phi}^{(l,e)}\boldsymbol{v}^{(l,e)}-\mathbf{G}^{(0,h)}\otimes\mathbf{T}_l\,\boldsymbol{u}^{(l,h)}+\sum_{m=1}^{l_*}\mathbf{\Psi}_m^{(l,e)}\boldsymbol{u}^{(m,e)}=\boldsymbol{b}_4^{(l)}, \tag{25}$$

where $\mathbf{G}^{(l,h)}$ is an $N \times N$ matrix with (i,j) entry given by

$$\mathbf{G}^{(l,h)}(i,j)=\frac{1}{\varepsilon^{(l)}(z_i)}\frac{d\phi_j^{(l,h)}}{dz}(z_i),$$

$\mathbf{\Phi}^{(l,e)}$ and $\mathbf{\Psi}_m^{(l,e)}$ can be defined by switching the polarization index from h to e in Eqs. (23) and (24).

Putting Eqs. (19), (20), (22) and (25) together, we obtain $4NM_l$ rows of Eq. (17) corresponding to the right hand side $\boldsymbol{b}^{(l)}$. The final system is obtained by repeating l from $l = 1$ to $l = l_*$. After Eq. (17) is solved, we use expansions (12) and (10) to construct $V_j^{(l,p)}$ and $V_j^{(0,p)}$ in the interior domain Ω_l ($l > 0$) and exterior domain Ω_0, respectively. The total field is then available through the vertical mode expansions (2), (3), (5) and (6). The scattering field can be calculated by subtracting $\{\mathbf{E}^{(0)}, \mathbf{H}^{(0)}\}$, the 1D solution in the exterior region S_0, from the total field.

In an early work [19], Boscolo and Midrio studied a dielectric slab with a finite number of holes for applications related to photonic crystal slabs. They analyzed the scattering of a guided mode of the slab by the holes using similar vertical mode and horizontal cylindrical wave expansions. Their expansions do not contain the 1D solutions, i.e., the terms $H_z^{(l)}$, $E_z^{(l)}$, $H_\tau^{(l)}$ and $E_\tau^{(l)}$ in (2), (3), (5) and (6). Therefore, their method cannot be used to analyze the scattering of an incident wave specified in the top or bottom homogeneous media. In addition, these authors choose to solve the coefficients of the cylindrical wave expansions (10) and (12). Although this seems very natural, it requires extensive manipulation of Bessel and Hankel functions using Graf's addition formulas. We choose to separate the vertical mode expansions given in Section 3 from the horizontal cylindrical wave expansions given in Section 4, and introduce the notion of DtN maps. This makes our method more general, since the DtN maps may be constructed by different methods. In [18], VMEM has been extended to single cylindrical structures with arbitrary cross sections where analytic solutions such as the cylindrical waves are not available. Boundary integral equations (BIEs) for 2D Helmholtz equations are used to implement the VMEM of [18]. There is no difficulty to extend that variant of VMEM with BIEs to structures with multiple cylinders of arbitrary cross sections, but for circular cylinders considered in this paper, our method based on the cylindrical wave expansions is certainly more efficient.

6. Numerical examples

In this section, we present some numerical examples to validate and illustrate our method. First, we follow Wang *et al.* [22], consider dimers and trimers consisting of silicon cylinders in free space. The radius and height of the cylinders $a = 120\,\text{nm}$ and $D = 240\,\text{nm}$, respectively. The refractive index of silicon is taken from the optical handbook of Palik [23]. The medium is nonmagnetic, thus $\mu = 1$ everywhere. Since the silicon cylinders are surrounded by free space, we have $\varepsilon_t = \varepsilon_b = \varepsilon^{(0)} = 1$. The incident wave is a normal incident plane wave propagating in the $-z$ direction.

For a dimer, we assume the centers of the cylinders are located on the x axis at $x = \pm(a + g/2)$, where g is the gap between the two cylinders. In Fig. 2, we show the scattering spectra of a dimer with $g = 200\,\text{nm}$ for a number of incident waves. The scattering properties depend on the relative orientation of incident electric field with respect to the dimer axis i.e., the x axis shown in the inset of Fig. 2. The four curves in Fig. 2 correspond to different values of θ, where θ is the horizontal angle between the incident electric field and the dimer axis. The existence of two resonant modes are evident from Fig. 2. These are the magnetic and electric resonant modes at longer and shorter wavelengths, respectively. When the angle θ is varied from 0 to $\pi/2$, the amplitude of the magnetic resonant mode decreases, and that of the electric resonant mode increases. As the gap between the two cylinders is reduced, the resonant wavelengths of these two modes move closer to each other. In Fig. 3, we show the scattering spectra of a silicon dimer with $g = 20\,\text{nm}$ for a normal incident wave with an electric field parallel to the dimer axis.

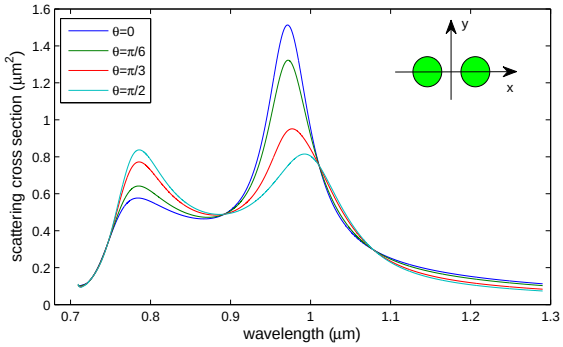

Fig. 2. Scattering spectra of a silicon dimer with a 200 nm gap for normal incident plane waves, where θ is the angle between the incident electric field and the x axis.

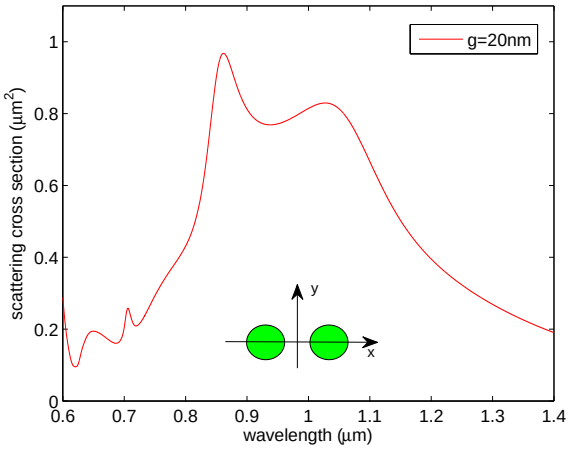

Fig. 3. Scattering spectra of a silicon dimer with a 20 nm gap for a normal incident wave with an electric field parallel to the x axis.

We also consider a trimer of three silicon cylinders with their centers forming an equilateral triangle in the xy plane. More specifically, we assume the centers of two cylinders are located on the x axis as the dimer before, and the center of the other cylinder is located on the y axis at $y = \sqrt{3}(a + g/2)$, where g is the gap between any two cylinders. In Fig. 4, we shows the scattering

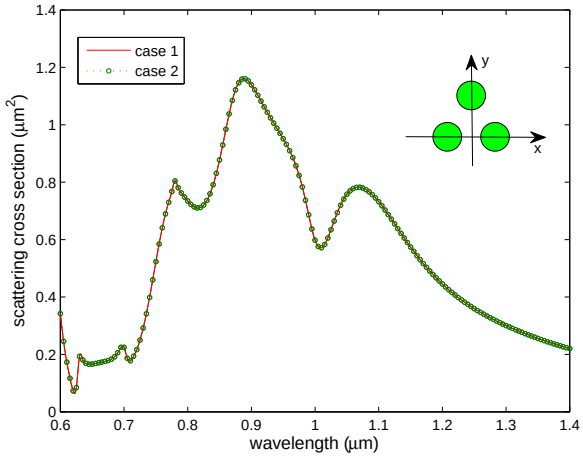

Fig. 4. Scattering spectra of a silicon trimer with a 60 nm gap for normal incident plane waves, where the electric field is parallel to the x axis (case 1) or to the y axis (case 2).

spectra of a trimer with $g = 60$ nm for two incident waves. It appears that the interaction of three cylinders brings in more complexity in the scattering behavior. The two cases in Fig. 4 correspond to incident waves with their electric field parallel or perpendicular to the x axis. It can be seen that the spectra responses for the two polarizations are almost identical for this structure. It seems that the increased symmetry of the trimer gives rise to a certain degree of robustness with respect to the polarization of the incident wave.

Our results shown in Figs. 2-4 agree with the FDTD results reported in [22]. In our calculations, we have used $N = 56$ points to discretize the z variable and $M_l = 9$ points to discretize horizontal boundary of each cylinder. For the trimer, we have $M = 3M_l = 27$, thus the final linear system involves $4NM = 6048$ unknowns, and it can be easily solved by a standard method based on Gaussian elimination. For problems with more particles, it is necessary to use an iterative method to solve the final linear system.

Next, we use the new VMEM to analyze metallic nanoparticles on a substrate. Following the early work of Rechberger *et al.* [2], we consider a dimer of two gold cylinders with radius $a = 75$ nm and height $D = 17$ nm, assuming the substrate is given in the entire half space $z < 0$ and has a refractive index 1.5, and the medium above the substrate is air. In this case, $\varepsilon_b = 1.5^2$, $\varepsilon_t = 1$ and $\mu = 1$ everywhere. The optical constant of gold is taken from [24].

In Fig. 5, we show the scattering properties of the

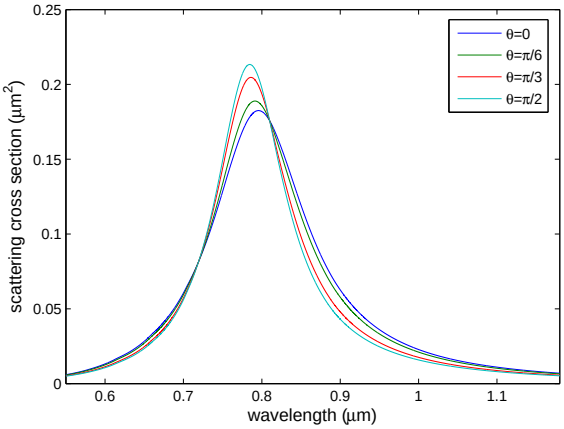

Fig. 5. Scattering spectra of a gold dimer with a 200 nm gap for a number of normal incident plane waves.

gold dimer for a fixed gap $g = 200$ nm. The different curves in Fig. 5 correspond to different polarization of the normal incident plane wave. As before, θ is the horizontal angle between the incident electric field and the dimer axis. Unlike the silicon dimer, the gold dimer has only one electric resonant mode in the visible and infrared frequency range. We also consider the dimer for different values of the gap g. In Fig. 6, we show the

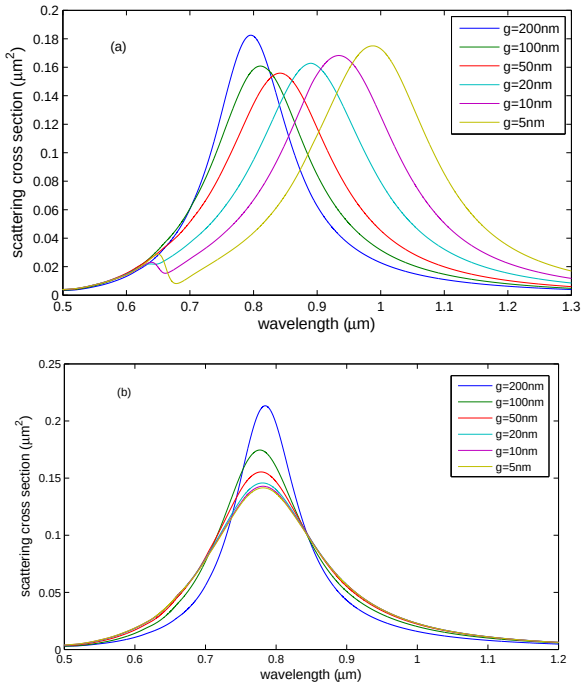

Fig. 6. Scattering spectra of a gold dimer with different values of the gap for normal incident plane waves, where the electric field is parallel (panel (a)) or perpendicular (panel (b)) to the dimer axis.

scattering spectra for $g = 200$, 100, 50, 20, 10 and 5 nm, respectively. Figure 6(a) and (b) correspond to incident waves with the electric field parallel and perpendicular to dimer axis, respectively. As the gap g is decreased, a remarkable redshift of the surface plasmon resonance wavelength can be seen in Fig. 6(a) for the parallel case. For the perpendicular case, one can observe a smaller blueshift in Fig. 6(b). The striking difference was observed in experiments by Rechberger *et al.* [2], and also appears in elliptic and other dimer structures [3, 4].

For the dimer with a 5 nm gap and the case corresponding to Fig. 6(a), a resonance occurs at freespace wavelength 0.99 μm. In Fig. 7, we show the magnitudes of E_x and E_y, normalized by the amplitude of the incident wave, on a horizontal plane at the middle of the nanoparticles for the resonant wavelength. Notice that

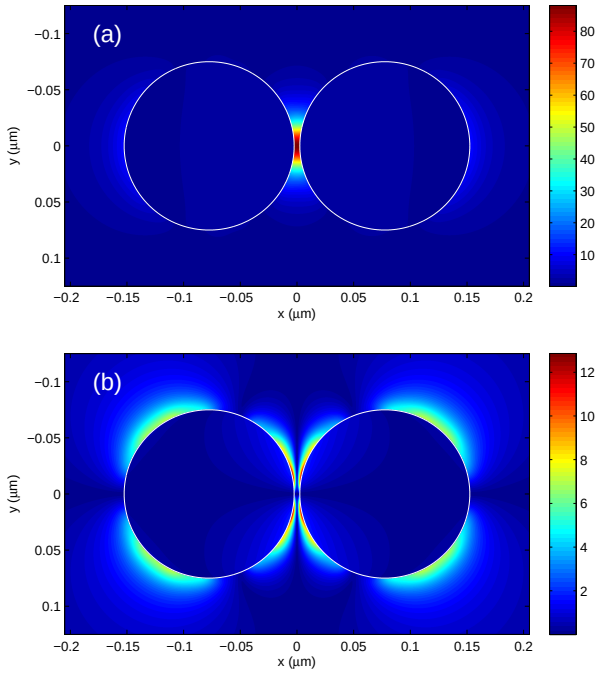

Fig. 7. Horizontal electric field components on the middle horizontal plane of a gold dimer with a 5 nm gap, for an incident plane wave with an electric field parallel to the dimer axis: (a) normalized $|E_x|$, (b) normalized $|E_y|$.

the E_x component is strongly enhanced in the gap. The E_y component is weaker, since the scales in the two plots are different. In Fig. 8, we show the normalized $|E_x|$ along the x axis on the same horizontal plane. In the gap, $|E_x|$ is much larger than the magnitude of the incident wave. The maximum of the normalized $|E_x|$ is about 88. This is consistent with the results on field enhancement in the gaps of similar gold dimers [25].

For the results shown in Figs. 5, 6 and 7, we discretize z by $N = 56$ points and discretize the circles Γ_l by $M_l = 19$ points. The final linear system involves 8512 unknowns, and it can be easily solved, since the coefficient matrix has many zero entries.

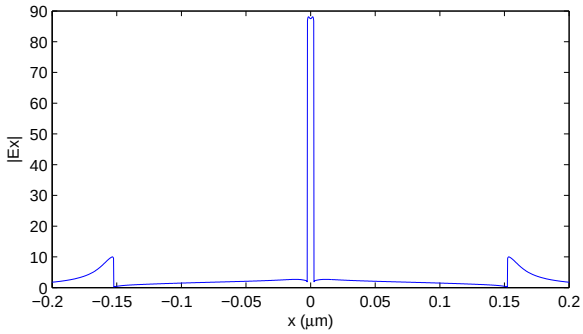

Fig. 8. Normalized $|E_x|$ along the x axis on the middle horizontal plane of a gold dimer.

7. Conclusions

The VMEM developed in the previous sections can be used to analyze the scattering of an incident wave by a finite number of circular cylindrical objects in a layered background. We have validated and illustrated the method using examples involving circular cylindrical nanoparticles in free space or on a substrate. The method is relatively efficient, since it avoids the discretization of 3D computational domains, and solves a linear system established on 2D boundaries of the 3D cylindrical regions. Compared with the boundary element method [10, 11] which is also formulated on a surface, VMEM has the advantage of simplicity, can easily handle layered background media, but it is more restrictive. Due to the special circular geometry of the cylinders, we make use of the analytic solutions for 2D Helmholtz equations that appear in the vertical mode expansion process. A more general VMEM can be developed by extending the method for a single cylinder of arbitrary cross section [18] to multiple cylinders. Despite of the restrictions, we believe the VMEM of this paper is useful, since circular cylinderical nanoparticles appear widely in experiments due to the relative simplicity of their fabrications, and practical applications require intensive numerical simulations for plasmonic structures with multiple nanoparticles.

Acknowledgments

This work was partially supported by the Research Grants Council of Hong Kong Special Administrative Region, China, under project CityU 11301914.

References

[1] M. Pelton and G. Bryant, *Introduction to Metal-Nanoparticle Plasmonics* (John Wiley & Sons, 2013).

[2] W. Rechberger, A. Hohenau, A. Leitner, J. R. Krenn, B. Lamprecht, and F. R. Aussenegg, "Optical properties of two interacting gold nanoparticles," Opt. Commun. **220**, 137–141 (2003).

[3] K.-H. Su, Q.-H. Wei, and X. Zhang, "Interparticle coupling effects on plasmon resonances of nanogold particles," Nano Lett. **3**(8), 1087–1090 (2003).

[4] T. Atay, J.-H. Song , and A. V. Nurmikko, "Strongly interacting plasmon nanoparticle pairs: from dipole-dipole interaction to conductively coupled regime," Nano Lett. **4**(9), 1627–1631 (2004).

[5] P. K. Jain, W. Huang, and M. A. El-Sayed, "On the universal scaling behavior of the distance decay of plasmon coupling in metal nanoparticle pairs: a plasmon ruler equation," Nano Lett. **7**, 2080–2088 (2007).

[6] G. Bachelier, I. Russier-Antoine, E. Benichou, C. Jonin, N. Del Fatti, F. Valle, and P.-F. Brevet, "Fano profiles induced by near-field coupling in heterogeneous dimers of gold and silver nanoparticles," Phys. Rev. Lett. **101**, 197401 (2008).

[7] A. Taflove and S. C. Hagness, *Computational Electrodynamics: the Finite-Difference Time-Domain Method*, 2nd ed. (Artech House, 2000).

[8] J. M. Jin, *The Finite Element Method in Electromagnetics*, 2nd ed. (John Wiley & Sons, 2002).

[9] W. C. Chew, M. S. Tong, and B. Hu, *Integral Equation Methods for Electromagnetic and Elastic Waves* (London: Morgan & Claypool, 2008).

[10] F. J. García de Abajo, "Retarded field calculation of electron energy loss in inhomogeneous dielectrics," Phys. Rev. B **65**, 115418 (2002).

[11] A. M. Kern and O. J. F. Martin, "Surface integral formulation for 3D simulations of plasmonic and high permittivity nanostructures," J. Opt. Soc. Am. A **26**, 732–740 (2009).

[12] L. Li, "New formulation of the Fourier modal method for crossed surface-relief gratings," J. Opt. Soc. Am. A **14**, 2758–2767 (1997).

[13] E. Silberstein, P. Lalanne, J.-P. Hugonin, and Q. Cao, "Use of grating theories in integrated optics," J. Opt. Soc. Am. A **18**, 2865–2875 (2001).

[14] G. Granet and J. P. Plumey, "Parametric formulation of the Fourier modal method for crossed surface-relief gratings," J. Opt. A **4**, S145–S149 (2002).

[15] V. Liu and S. Fan, "S^4: A free electromagnetic solver for layered periodic structures," Computer Physics Communications **183**, 2233–2244 (2012).

[16] K. B. Dossou, L. C. Botten, A. A. Asatryan, B. C. P. Sturmberg, M. A. Byrne, C. G. Poulton, R. C. McPhedran, and C. M. de Sterke, "Modal formulation for diffraction by absorbing photonic crystal slabs," J. Opt. Soc. Am. A **29**, 817–831 (2012).

[17] X. Lu, H. Shi, and Y. Y. Lu, "Vertical mode expansion method for transmission of light through a single circular hole in a slab," J. Opt. Soc. Am. A **31**, 293–300 (2014).

[18] H. Shi and Y. Y. Lu, "Efficient vertical mode expansion method for scattering by arbitrary layered cylindrical structures," Opt. Express **23**, 14618–14629 (2015).

[19] S. Boscolo and M. Midrio, "Three-dimensional multiple-scattering technique for the analysis of photonic-crystal slabs," J. Lightw. Technol. **22**, 2778–2786 (2004)

[20] M. J. Grote and C. Kirsch, "Dirichlet-to-Neumann boundary conditions for multiple scattering problems," J. Comput. Phys. **201**, 630–650 (2004).

[21] L. N. Trefethen, *Spectral Methods in MATLAB* (Society for Industrial and Applied Mathematics, 2000).

[22] C. Wang, Z. Y. Jia, K. Zhang, Y. Zhou, R. H. Fan, X. Xiong, and R. W. Peng, "Broadband optical scattering in coupled silicon nanocylinders," J. Appl. Phys. **115**, 244312 (2014).

[23] E. D. Palik, *Handbook of Optical Constants of Solids* (Academic, 1998).

[24] P. B. Johnson and R. W. Christy, "Optical constants of the noble metals," Phys. Rev. B **6**, 4370–4379 (1972).

[25] D. Sarid and W. Challener, *Modern Introduction to Surface Plasmons: Theory, Mathematical Modeling, and Applications*, Chapter 9 (Cambridge University Press, 2010).